

## Piezoelectric bimorph-based shear force microscopy for the construction of noble metal plasmonic structures in air

This content has been downloaded from IOPscience. Please scroll down to see the full text.

2015 Mater. Res. Express 2 075701

(<http://iopscience.iop.org/2053-1591/2/7/075701>)

View [the table of contents for this issue](#), or go to the [journal homepage](#) for more

Download details:

IP Address: 202.28.191.34

This content was downloaded on 01/01/2016 at 02:24

Please note that [terms and conditions apply](#).

# Materials Research Express



## PAPER

# Piezoelectric bimorph-based shear force microscopy for the construction of noble metal plasmonic structures in air

Wei Cai<sup>1,2</sup>, Mu Yang<sup>1</sup>, Yingjie Wang<sup>1</sup> and Guangyi Shang<sup>1,2</sup>

<sup>1</sup> Department of Applied Physics, Beihang University, Beijing 100191, People's Republic of China

<sup>2</sup> Key Laboratory of Micro-nano Measurement-Manipulation and Physics (Ministry of Education), Beihang University, Beijing 100191, People's Republic of China

E-mail: [gyshang@buaa.edu.cn](mailto:gyshang@buaa.edu.cn)

**Keywords:** shear force microscopy, micro/nano manipulation, plasmonic structure, bimorph-based shear force sensor

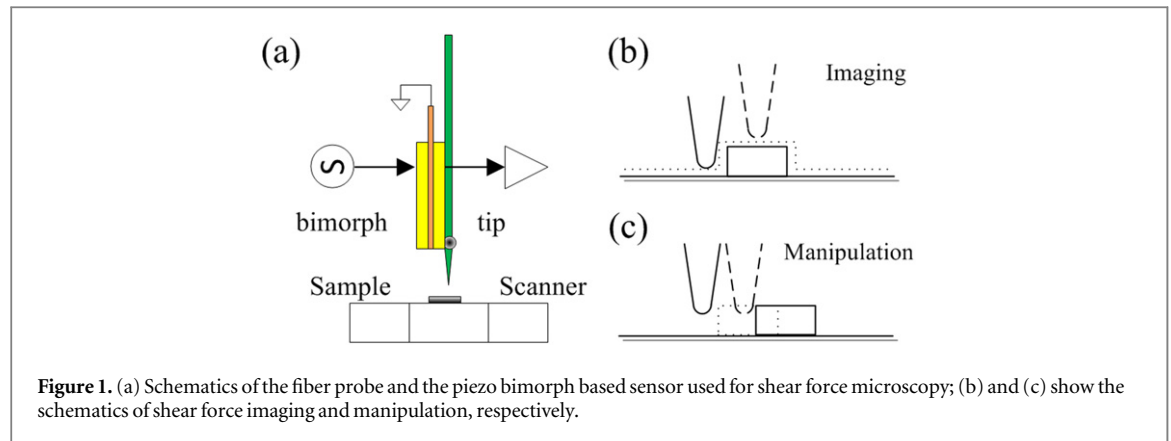
## Abstract

In this article, we present an alternative method to directly manipulate the noble metal structures in air. The method is carried out based on a home-made shear force microscope, which mainly consists of a fiber probe-bimorph beam shear force sensor, a scanning probe microscope controller, and a nano-positioning stage. The magnitude of the probe-sample interaction forces as a function of the set-point ratio is estimated, which shows that the magnitude of the forces is inversely proportional to the set-point ratio. The microscopic imaging and manipulation can be realized at the higher and lower set-point values, respectively. Typical results of imaging at the set-point ratio of larger than 90% and manipulation at that of lower than 60% are demonstrated. The results suggest that this method would provide a promising way to study the relation between plasmonic structures and optical properties on the micro/nano scale.

## 1. Introduction

It has been known that noble metal structures show fascinating optical properties due to surface plasmon polaritons (SPPs) and/or localized plasmon polaritons, which can guide the light propagation direction and/or enable the light localization [1]. Since the wavelength of SPPs excited on plasmonic structures is shorter than that of the exciting light, the dimensions of the structure can be reduced to sub-wavelength scale [2]. By means of electron-beam lithography and focused ion beam milling methods, various plasmonic structures have been fabricated on the noble metal films [3]. In addition, theoretical and experimental studies on plasmonic structures have already led to a great number of applications in the fields of the next generation integrated optical circuits [4, 5], chemical/bio-sensors [6–8], and solar cells [9–11] etc. However, the structure parameters (e.g. the space or the position) and their corresponding optical properties cannot be changed if the fabrication processes are finished.

In order to *in situ* tune the optical properties of plasmonic structures, great efforts have been made and a number of methods have been developed. For example, the graphene-based structure is of particular interest to researchers. The optical properties of graphene can be tuned or controlled via the gate voltage [12, 13]. The methods to tune the optical properties without the voltage control have also been realized. Atomic force microscopy (AFM) based methods have been used to directly manipulate the structure parameters of the particles for tuning the optical properties [14]. Tong *et al* utilized AFM to manipulate the gold nanoparticles [15], where the highest field enhancement for Raman spectroscopy was found in the linear structure of closely spaced particles. Optical tweezers or trapping methods have the ability to finely control individual nano- and micro-objects [16]. Zhang *et al* proposed a plasmonic antenna based optical trapping method [17]. Optical properties (scattering spectra) of the antennas would be changed if nanoparticles were trapped in the antennas. Recently, Brian *et al* developed a method based on the electron-beam [18]. By controlling the accelerating voltage and the scan area, the electron-beam-induced gradient forces will be changed and thus the gap size of the antenna can be adjusted [19]. These methods provide us with direct means to reconfigure the plasmonic



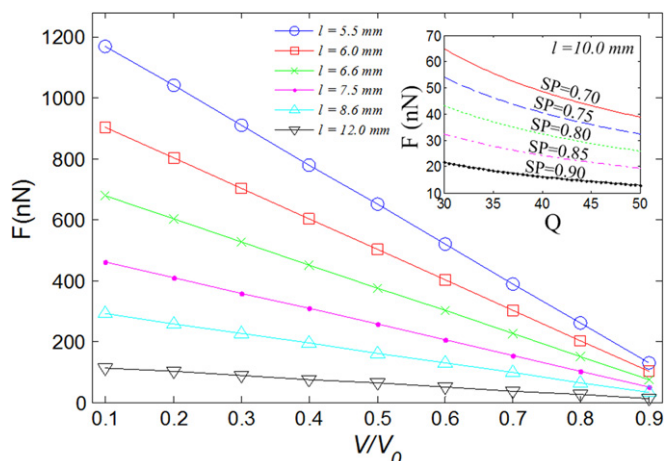
structure. Unfortunately, when AFM method is used for manipulation, the feedback loop has to be switched off [20, 21] and careful operation is needed to avoid the tip scratching the sample surface. Optical trapping method requires liquid environment [17, 22] due to the small optical force. For the electron-beam method, vacuum environment is necessary.

In this article, we propose an alternative method to directly manipulate plasmonic structures. By using piezoelectric bimorph-based shear force microscopy, both imaging and manipulation operations in air can be realized. Two operations could be switched via carefully adjusting the set-point ratio of the amplitude feedback. In imaging operations, topographic images of both the hard sample (a calibration grating) and the soft sample (a DNA test sample) were obtained by using the shear force method, respectively. In manipulation one, silver plates and rods prepared for plasmonic structures were then directly manipulated. The results indicate that this method can not only realize microscopic imaging with nanometer resolution but also provide an effective way to manipulate the structure parameters in air. It would be a promising method to study the relation between plasmonic structures and optical properties on the micrometer or even nanometer scale.

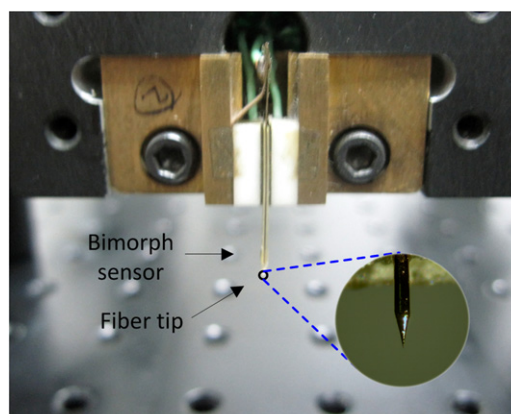
## 2. Method

Figure 1(a) shows a schematic of the fiber probe and piezo bimorph-based sensor used for shear force imaging and manipulation method. The sensor consists of a fiber probe and a bimorph beam. The fiber probe is attached on one side of the bimorph beam with superglue. The tip free length is usually  $\sim 0.5\text{--}1$  mm. One piezo layer of the bimorph is used for driving the tip to vibrate parallel to the sample surface. The driving frequency is set at the fundamental resonance peak of the bimorph beam. The other piezo layer is the sensing layer, which provides the signals to monitor the vibration. Once the tip interacts with the sample surface, the vibration signals will vary correspondingly [23, 24]. In imaging operations, as shown in figure 1(b), amplitude feedback is used to regulate the tip-sample distance for keeping the oscillation amplitude as a constant. The feedback voltage to z-axis of the piezo scanner, which helps the tip to track the sample surface, is recorded as the height signal. A relative larger set-point ratio (set-point amplitude/free oscillation amplitude) is used in order to decrease the tip-sample interactions. High quality shear force topographic images can be obtained in this way. In manipulation operations, in case of stable feedback loop, the relative lower set-point ratio means that the tip will get closer to the surface and thus the net interaction forces will be increased. If the magnitude of the tip-sample interaction forces exceeds the friction/adhesion force between the sample and the substrate, the sample will be 'pushed' by the dithering tip, as shown in figure 1(c). However, if the set-point ratio is too low, the tip and/or the sample surface will be damaged.

The mechanical behavior of the fiber probe-bimorph assembly would be dominated by the bimorph cantilever [23]. The spring constant of the cantilever can be calculated by  $K_c = Ewt^3/4l^3$ , where  $E$ ,  $w$ , and  $t$  is Young's modulus, the width, and the thickness of the bimorph cantilever, respectively.  $l$  is the length of the cantilever that can be finely adjusted during the clamping process. Higher spring constant  $K_c$  of the cantilever can be obtained with smaller cantilever length  $l$ . The magnitude of interaction forces between the tip and the sample can be evaluated by  $F_s = (1 - V/V_0)K_c x_0 / (\sqrt{3}Q)$  [25], where  $V/V_0$  is the set-point ratio,  $x_0$  is the amplitude of free oscillation which can be measured by the optical lever method [26] and is typically a few nanometers [27]. The quality factor  $Q$  can be obtained from the resonance curve by Lorentzian curve fit. Figure 2 gives the relations between the set-point ratio and the estimated force by above formulas with different cantilever length  $l$ . If the length  $l$  is fixed, a larger set-point ratio (close to 95%) will keep interaction forces at a small level ( $\sim 10$  nN when  $l = 10$  mm) during imaging. On the contrary, interaction forces will increase if using a smaller



**Figure 2.** The relations between the set-point ratio and the interaction force evaluated by the formulas with different cantilever length  $l$ , calculated with parameters of Young's modulus  $E = 5.2 \times 10^{10} \text{ N m}^{-2}$ , the width  $w = 2 \text{ mm}$ , the thickness of the cantilever  $t = 0.6 \text{ mm}$ , the amplitude of free oscillation  $x_0 = 2 \text{ nm}$ , and quality factor  $Q = 30$ . The inset figure shows the relations between the  $Q$ -factor and the interaction force. The length  $l$  is set to  $10 \text{ mm}$ . The set-point (SP) ratio varies from  $0.70$  to  $0.90$ .



**Figure 3.** A photograph of the fiber tip and the bimorph sensor used for shear force imaging and manipulation. The inset photograph shows a fiber tip fabricated by chemical etching method.

set-point ratio. The inset figure shows the relations between the  $Q$ -factor and the interaction forces. In experiments,  $Q$ -factor typically related to the mass of the glue. If the cantilever length and the set-point ratio are fixed, larger  $Q$ -factor would ensure sufficient sensitivity during imaging, but relative smaller  $Q$ -factor would result in larger force during manipulation. Therefore, there is a trade-off between imaging and manipulation operations and the sensor can be designed before experiments.

### 3. Experimental setup

Figure 3 shows a photograph of the fiber probe-bimorph sensor used for shear force imaging and manipulation. The bimorph sensor is clamped by a specially designed holder and arranged in vertical direction relative to the sample surface. A typical image of the fiber tip fabricated by chemical etching method is shown in the inset. The pretreated fiber has a diameter of  $125 \mu\text{m}$  and the typical tip apex size is  $\sim 100 \text{ nm}$  [28, 29].

Beside the shear force sensor, our system also includes a scanning probe microscope (SPM) controller (Benyuan CSPM 5000, China), a three-dimensional piezo nanopositioning stage (Physik-Instrumente PI.517, 3CL, Germany), a lock-in amplifier (DSP 7265, Ametek, USA), and an inverted optical microscope (XDS-1, Chongqing Optical Instrument Factory, Chongqing, China) equipped with a long distance objective (SLMPlan, 50X/0.45, WD =  $15 \text{ mm}$ , Olympus, Japan). The other end of the fiber tip is cleaved and coupled to a  $532 \text{ nm}$  laser diode. When the tip is engaged to the sample surface, the emitted light from its tip apex can be monitored by the inverted optical microscope, which can be used to indicate the position of the tip in the  $x$ - $y$  plane.

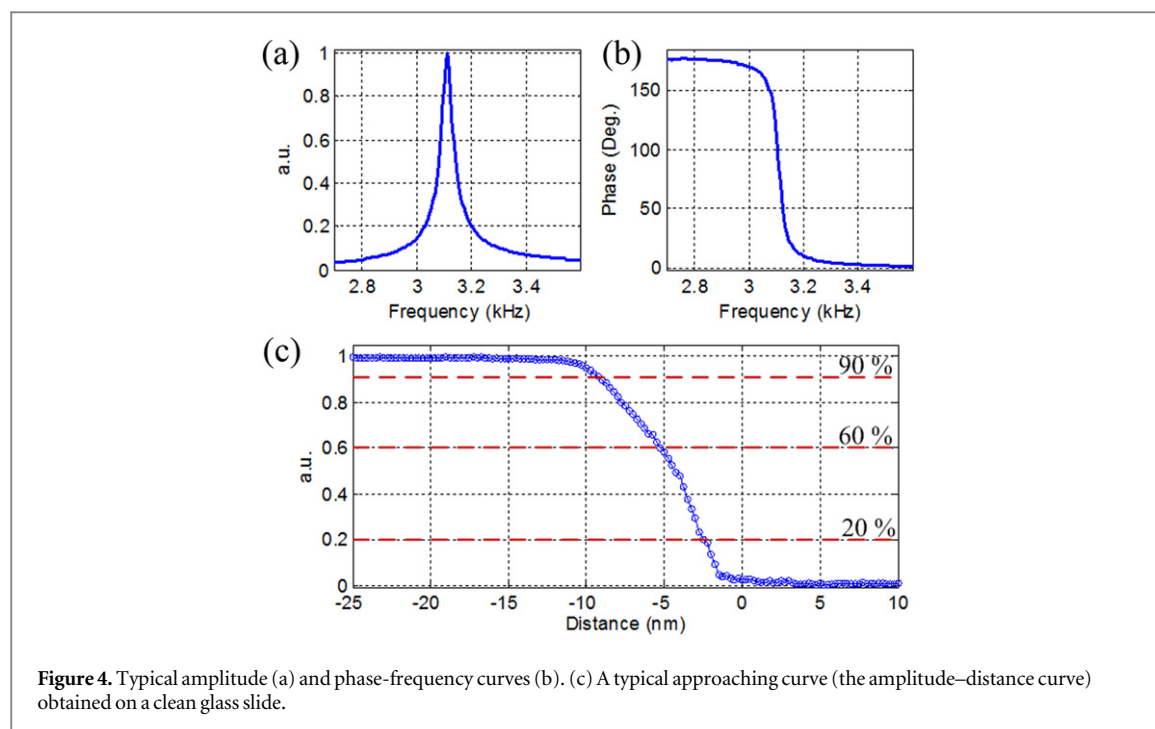


**Figure 4.** Typical amplitude (a) and phase-frequency curves (b). (c) A typical approaching curve (the amplitude–distance curve) obtained on a clean glass slide.

Silver plates with average thickness of 20–30 nm and average size tunable from several hundreds of nanometers to several micrometers have been synthesized for plasmonic structures via a chemical method [30]. A drop of the sample was placed onto a clean glass slide, and then air dried. The density of particles on the slide is controlled to be less than 5 particles/ $\mu\text{m}^2$ . Observed by the optical microscope, typical shapes of the plates are triangle and hexagon. The rod-like shape can also be found.

#### 4. Results and discussions

Figures 4(a) and (b) show typical resonance and phase-frequency curves of the shear force sensor, respectively. The resonance frequency is  $\sim 3.1$  kHz and the  $Q$ -factor  $\sim 30$ . Figure 4(c) gives a typical amplitude approaching curve measured with a glass slide in air. The driving frequency is set at the resonance peak of the bimorph cantilever. The feedback loop of  $z$ -axis of the scanner needs to be switched off during the measurement of the approaching curves. The first point where the amplitude signal gets to the minimum value is defined as the zero point of the approaching curve. From this curve we can find out that once the tip is approached, a drastically decreased amplitude signal would be observed in the range of  $\sim 15$  nm to the sample surface due to the tip–sample shear force interactions [30]. In our experiments, for imaging operations, the set-point value is usually set higher than 90% of the free oscillation amplitude. And for manipulation operations, the set-point value has been lowered to  $\sim 60\%$  of the free oscillation amplitude. Finely adjusting the set-point value is necessary according to the friction force between the sample and the substrate. However, if the set point ratio is too low, typically  $< 20\%$ , it was found that the tip and/or the sample surface will be damaged.

Figure 5 shows the typical images obtained by the bimorph shear-force sensor working in imaging operations. Figure 5(a) gives an image of a standard silicon calibration grating (TGZ1, NTMDT, Russia) with a period of  $3\ \mu\text{m}$  and height of  $\sim 20$  nm. The scan size is  $\sim 12.5\ \mu\text{m}$ , the set-point ratio is 92%, and the scan rate is 0.5 Hz. From this image, the morphology of the grating and some fine structures can be seen clearly. To demonstrate the imaging sensitivity of the bimorph sensor, figure 5(b) gives the image of the DNA test sample (DNA01, NTMDT, Russia). The scan size is  $\sim 700$  nm, the set-point ratio is 95%, and the scan rate is 0.3 Hz. Linear DNA molecules can be distinguished from this topographic image.

During experiments, the manipulation processes were performed in the following way. First, the tip was engaged with a larger set-point ratio and then located near the object of interest with the help of the laser emitted from the fiber tip. Because once the tip was in the near-field of the surface, the laser spot can be seen in the view of the inverted optical microscope, thus the position of the tip can be marked. Then, the set-point ratio was lowered about 5% of the free oscillation amplitude (e.g. from 90%  $V_0$  to 85%  $V_0$ ). In the case, the object could be moved toward the tip by adjusting the offset voltage of the nano-positioning stage. The velocity of the movement was smaller than that of scanning for imaging. If the object was not moved, lowered the set-point value  $\sim 5\%$  of the free oscillation amplitude again and repeated the steps until the position of the object was changed.



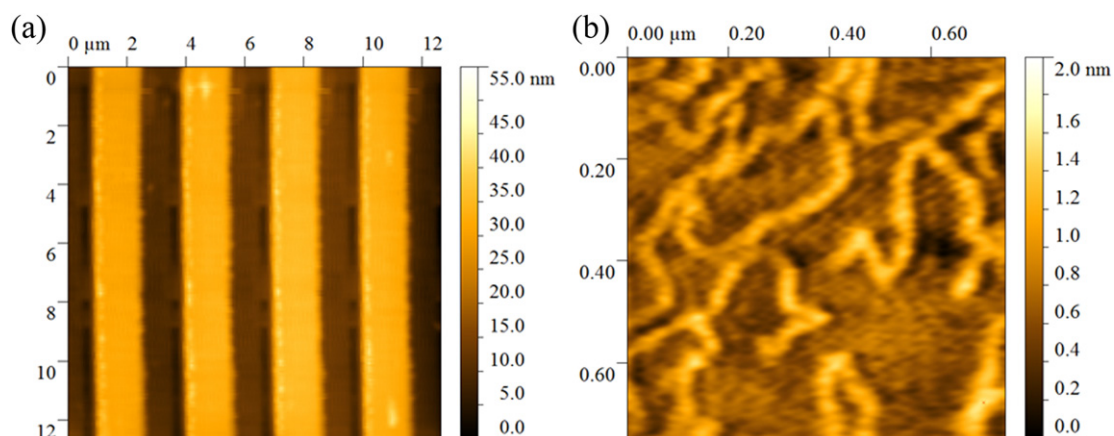


**Figure 5.** Shear force topographic images of the silicon calibration grating (a) and the DNA test sample (b). The scan size is  $\sim 12.5 \mu\text{m}$  and  $\sim 700 \text{ nm}$ , respectively.

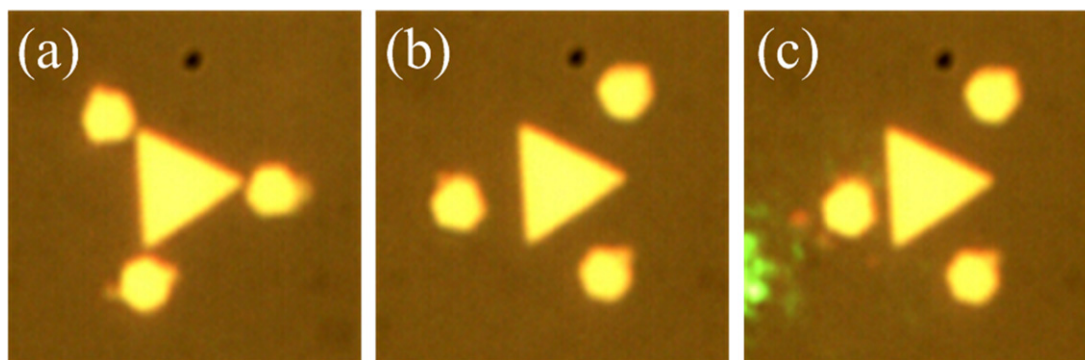


**Figure 6.** One example of the direct manipulation of the silver plates by our method. (a)–(c) Shows that three small hexagon plates' positions can be moved to the new positions near the three vertices (a) and sides (b) of a bigger triangle plate. The distance between one hexagon plate and the triangle plate can be further regulated as shown in (c). These optical microscopy images have a size of  $\sim 10 \mu\text{m}$ .

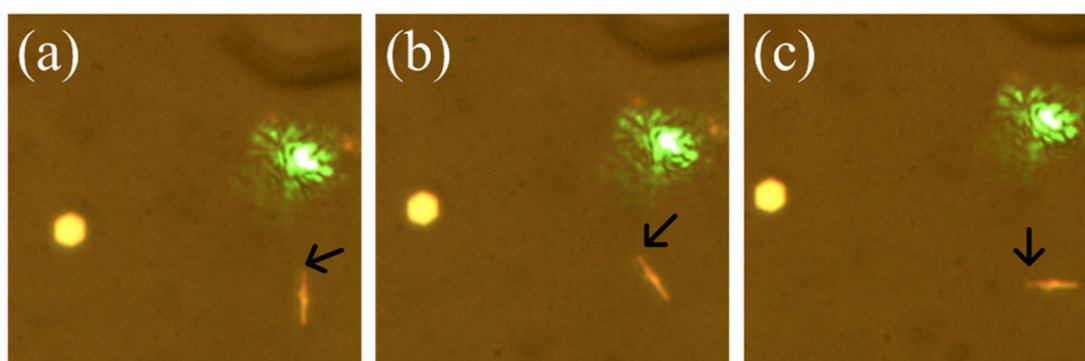


**Figure 7.** The other example of direct manipulation of a silver rod by our method. By carefully adjusting one end of the rod toward to the tip, the orientation of the silver rod can be changed. The arrow in each figure indicates the tip's moving direction. These optical microscopy images have a size of  $\sim 20 \mu\text{m}$ .

Figures 6(a)–(c) show an example of the manipulation of the silver plates. It was found that most of particles with the size of  $\sim 1 \mu\text{m}$  on the glass slide can be moved when the set-point ratio reduced to  $\sim 55\%$ . As shown in figure 6(a), by using this method, the position of three small hexagon plates can be adjusted to the new positions closed to the three vertices of a bigger triangle plate. Then, three hexagon plates can be moved in the same way to the three sides of the triangle plate, as shown in figure 6(b). Moreover, the distance between one hexagon plate

and the triangle plate can be further regulated in figure 6(c), indicating that the structure can be changed if *in situ* adjustment of the optical properties is needed. These images have a size of  $\sim 10\ \mu\text{m}$ .

Figures 7(a)–(c) show another example of the direct manipulation of a rod-like silver plate using our method. The laser spot represents the position of the tip. By carefully adjusting one end of the rod towards the tip, the orientation of the silver rod can be changed. The hexagonal shape in the given images is a silver plate as a position reference. The center position of the rod has a little offset during manipulation. The size of these images is  $\sim 20\ \mu\text{m}$ . The set-point ratio is 55% in manipulation. To verify that the tip was not damaged during manipulation of the silver plates, a piece of optical disk with periodicity of  $1.6\ \mu\text{m}$  was imaged. Good and repeatable images were obtained, implying that the tip was not damaged.

## 5. Conclusion

In summary, we present an alternative method to directly manipulate the structure parameters of plasmonic structures. Based on the piezoelectric bimorph shear force sensor, the system for shear force imaging and manipulation has been built. The imaging and manipulation operations can be switched by carefully adjusting the set-point ratio of the amplitude feedback. Topographic images of both the hard sample (a calibration grating) and the soft sample (a DNA test sample) were obtained by using the shear force imaging method, respectively. In manipulation operations, silver micro-plates with various shapes were directly rearranged. Our on-going work has focused on the detection of the optical properties of plasmonic structures by means of shear force microscope and near-field optical microscope. Nevertheless, the method would provide a promising way to construct the plasmonic structures and study plasmonic phenomena of various structures.

## Acknowledgments

This work was supported by the China National Key Basic Research Program 973 (Grant No. 2013CB934004), the National Natural Science Foundation of China (Grant No. 11232013, 11304006), and the Fundamental Research Funds for the Central Universities (Grant No. YWF-13-D2-XX-14).

## References

- [1] Maier S A and Atwater H A 2005 Plasmonics: localization and guiding of electromagnetic energy in metal/dielectric structures *J. Appl. Phys.* **98** 011101
- [2] Pelton M, Aizpurua J and Bryant G 2008 Metal-nanoparticle plasmonics *Laser Photon. Rev.* **2** 136–59
- [3] Henzie J, Lee J, Lee M H, Hasan W and Odom T W 2009 Nanofabrication of plasmonic structures *Annu. Rev. Phys. Chem.* **60** 147–65
- [4] Ozbay E 2006 Plasmonics: merging photonics and electronics at nanoscale dimensions *Science* **311** 189–93
- [5] Gramotnev D K and Bozhevolnyi S I 2010 Plasmonics beyond the diffraction limit *Nat. Photonics* **4** 83–91
- [6] Stewart M E, Anderton C R, Thompson L B, Maria J, Gray S K, Rogers J A and Nuzzo R G 2008 Nanostructured plasmonic sensors *Chem. Rev.* **108** 494–521
- [7] Anker J N, Hall W P, Lyandres O, Shah N C, Zhao J and Van Duyne R P 2008 Biosensing with plasmonic nanosensors *Nat. Mater.* **7** 442–53
- [8] Aristov A I, Zywiets U, Evlyukhin A B, Reinhardt C, Chichkov B N and Kabashin A V 2014 Laser-ablative engineering of phase singularities in plasmonic metamaterial arrays for biosensing applications *Appl. Phys. Lett.* **104** 071101
- [9] Atwater H A and Polman A 2010 Plasmonics for improved photovoltaic devices *Nat. Mater.* **9** 205–13
- [10] Spinelli P, Ferry V, Van de Groep J, Van Lare M, Verschuuren M, Schropp R, Atwater H and Polman A 2012 Plasmonic light trapping in thin-film Si solar cells *J. Opt.* **14** 024002
- [11] Bhattacharya J, Chakravarty N, Pattnaik S, Dennis Slafer W, Biswas R and Dalal V L 2011 A photonic-plasmonic structure for enhancing light absorption in thin film solar cells *Appl. Phys. Lett.* **99** 131114
- [12] Grigorenko A, Polini M and Novoselov K 2012 Graphene plasmonics *Nat. Photonics* **6** 749–58
- [13] Jablan M, Soljacic M and Buljan H 2013 Plasmons in graphene: fundamental properties and potential applications *Proc. IEEE* **101** 1689–704
- [14] Rubio-Sierra F J, Heckl W M and Stark R W 2005 Nanomanipulation by atomic force microscopy *Adv. Eng. Mater.* **7** 193–6
- [15] Tong L, Zhu T and Liu Z 2008 Atomic force microscope manipulation of gold nanoparticles for controlled Raman enhancement *Appl. Phys. Lett.* **92** 023109
- [16] Veiga-Gutiérrez M, Woerdemann M, Prasetyanto E, Denz C and De Cola L 2012 Optical-tweezers assembly-line for the construction of complex functional Zeolite L structures *Adv. Mater.* **24** 5199–204
- [17] Zhang W, Huang L, Santschi C and Martin O J 2010 Trapping and sensing 10 nm metal nanoparticles using plasmonic dipole antennas *Nano Lett.* **10** 1006–11
- [18] Roxworthy B J, Bhuiya A M, Yu X, Chow E K and Toussaint K C Jr 2014 Reconfigurable nanoantennas using electron-beam manipulation *Nat. Commun.* **5** 4427
- [19] Vesseur E J R, Aizpurua J, Coenen T, Reyes-Coronado A, Batson P E and Polman A 2012 Plasmonic excitation and manipulation with an electron beam *MRS Bull.* **37** 752–60
- [20] Junno T, Deppert K, Montelius L and Samuelson L 1995 Controlled manipulation of nanoparticles with an atomic force microscope *Appl. Phys. Lett.* **66** 3627–9

- [21] Martin M, Roschier L, Hakonen P, Parts Ü, Paalanen M, Schleicher B and Kauppinen E I 1998 Manipulation of Ag nanoparticles utilizing noncontact atomic force microscopy *Appl. Phys. Lett.* **73** 1505–7
- [22] Wang K, Schonbrun E, Steinvurzel P and Crozier K B 2011 Trapping and rotating nanoparticles using a plasmonic nano-tweezer with an integrated heat sink *Nat. Commun.* **2** 469
- [23] Shang G, Wang C, Wu J, Bai C and Lei F 2001 Shear force scanning near-field optical microscope based on a piezoelectric bimorph cantilever *Rev. Sci. Instrum.* **72** 2344–9
- [24] Shang G Y, Lei F H, Troyon M, Qiao W H, Trussardi-Regnier A and Manfait M 2004 Non-optical bimorph-based tapping-mode force sensing method for scanning near-field optical microscopy *J. Microsc.* **215** 127–30
- [25] Karrai K and Grober R D 1995 Piezoelectric tip-sample distance control for near field optical microscopes *Appl. Phys. Lett.* **66** 1842–4
- [26] Yaralioglu G, Atalar A, Manalis S and Quate C 1998 Analysis and design of an interdigital cantilever as a displacement sensor *J. Appl. Phys.* **83** 7405–15
- [27] Lei F H, Nicolas J-L, Troyon M, Sockalingum G D, Rubin S and Manfait M 2003 Shear force detection by using bimorph cantilever with the enhanced Q factor *J. Appl. Phys.* **93** 2236–43
- [28] Turner D R 1983 *U S Patent* (5 April)
- [29] Lazarev A, Fang N, Luo Q and Zhang X 2003 Formation of fine near-field scanning optical microscopy tips: I. By static and dynamic chemical etching *Rev. Sci. Instrum.* **74** 3679–83
- [30] Liang H, Wang W, Huang Y, Zhang S, Wei H and Xu H 2010 Controlled synthesis of uniform silver nanospheres *J. Phys. Chem. C* **114** 7427–31